AIAA 2013-5154

Geometry Based Flight Dynamics Modelling of Unmanned Airplanes

Andreas Klöckner*

This paper presents estimation algorithms for flight dynamics of small unmanned aircraft. The estimates are mainly based on geometric information. Optional information taken into account are airfoil polars, a few mass characteristics and static thrust measurements. The aerodynamics dataset is estimated using the Vortex Lattice Method. Weight-and-balance estimates are driven by assuming constant mass per surface. Propulsion is estimated based on typical characteristics. The model is compared to higher-fidelity models, namely wind-tunnel measurements and inertia measurements. The differences to the reference are typically below 20% of the aerodynamic coefficients and below 10% of the reference inertia.

I. Introduction

Flight dynamics simulation is needed for a wide range of applications in aeronautics. Flight control laws e.g. can be designed only, if the developer can predict the aircraft's behavior in response to the control inputs. As the flight dynamics may influence the quality of sensor data, its prediction is also necessary for the design of experiments. Proper mission planning is also not possible without knowledge of the aircrafts' performance and limitations. Typical UAV applications additionally become increasingly involved in coupling payload such as gimballed cameras or manipulators to the aircraft's flight dynamics, therefore also requiring knowledge of the aircrafts' behavior in flight.

For regular civil or military aircraft, engineers seek to create high-fidelity simulation models. Intensive numeric calculations and laborious experiments are conducted, in order to accurately predict aircraft behavior. Expensive equipment and man-power are needed to achieve this task.

On the one hand, these resources are usually not available for small research aircraft. The budget as well as the team are very small and the main focus of work is on the team's particular research subjects. Typical UAV laboratories additionally operate a multitude of very heterogeneous platforms with different configurations. Additionally, a research UAV's characteristics are very short-living, as different equipment is mounted in or on the airframe on a daily basis. Figure 1 e.g. illustrates the difference in aircraft configurations used at the DLR Robotics and Mechatronics Center, as well as the size of the team.

Figure 1. Different platforms used at the DLR Robotics and Mechatronics Center range from regular model aircrafts such as Frauke to the 25kg aircraft ELWIRA. The core team operating these aircraft includes about ten people.

On the other hand, research UAVs are usually operated in a very limited domain and in restricted airspace, such that extensive safety margins are not demanded. The fidelity level of the models can thus be lowered to a certain extent in favor of the estimations' flexibility, turn-around times, and usage of resource.

In summary, simple and flexible, yet reasonably accurate flight dynamics estimation routines are needed for UAV applications. These would, ideally, rely on a very simple set of input data, which is easy to

*Research Associate, German Aerospace Center, Institute of System Dynamics and Control, Münchner Straße 20, D-82234 Oberpfaffenhofen-Weßling.

determine. The present paper describes such an algorithm (see Sec. II) and provides a comparison to more realistic models (see Sec. III).

II. Flight Dynamics Estimation

The dynamics of a flying aircraft are governed by the fundamental proposition that all forces acting on its airframe are in equilibrium. These forces have three major contributions for typical, rigid-body aircraft: aerodynamics, inertia of mass and propulsion. The presented tool chain provides estimations for all three of these contributions. The algorithm is driven only by geometric data and some additional information, which is typically available for a model aircraft or can easily be measured. This is motivated by the fact that most current research UAVs are based on model aircraft platforms.

The algorithm's main input is a geometry description, which can be given in a plain text format used by the AVL software.[1] This file is directly used in an automated process to yield a simplified representation of the aerodynamic forces and moments from the AVL vortex lattice code. The approach is described in Sec. II.A. In Fig. 2, the geometry of the University of Minnesota's FASER aircraft[2] is shown. This aircraft is used as a benchmark for the aerodynamics estimation.

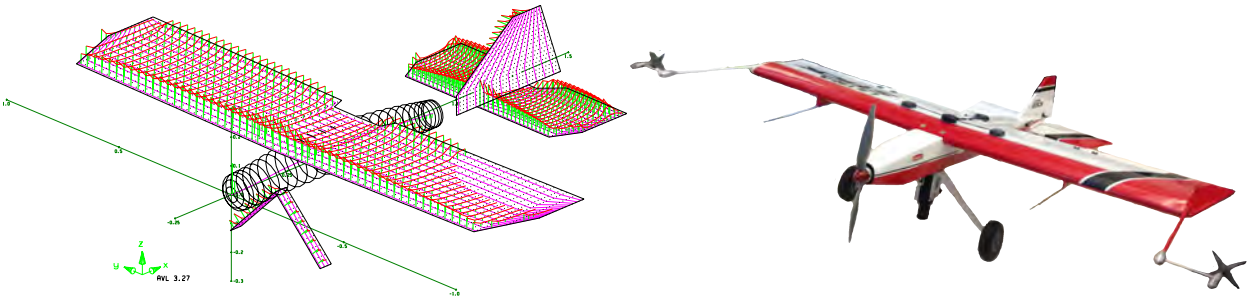

Figure 2. The core input to the flight dynamics estimation is the airframe's geometry described by an AVL mesh. The University of Minnesota's FASER airframe is used as a reference for validation. Its geometry is depicted here together with an examplary distribution of the aerodynamic forces and a photograph of the aircraft.

The same geometry description is used to estimate the mass distribution of the aircraft by evenly distributing the structural mass over the UAV's surface. The geometry can be supplemented by additional knowledge about distinct mass points and their location inside the airframe, such as payloads or batteries. It should also be supported by the measured overall center of gravity of the aircraft. This weight-and-balance module is described in Sec. II.B.

Propulsive forces are estimated for a model aircraft propeller by a simple combination of geometric parameters of the propeller and typical characteristics. They can, and should, be supported by static thrust experiments. The procedure is presented in Sec. II.C.

The output of the estimations is fed into a template based on the DLR Flight Dynamics Library.[3] The library provides the necessary infrastructure for six degrees of freedom (6DOF) simulation models of the aircraft. Positions can be expressed in the World Geodetic System (WGS84) and the rotation of the earth is taken into account. Detailed models of the magnetic and gravitational fields of the earth are included in the library as well as standard atmosphere data and wind simulation. The approach is very modular and can easily be extended by additional models of higher complexity than shown here.[4]

A major advantage of the Flight Dynamics Library is that it is based on the Modelica equation-based modelling language.[5] This allows for bidirectional data flow between the modules. The simulation's level of detail can easily be switched without the need to change the model equations manually. The models can even be automatically inverted in the sense of non-linear dynamic inversion for mission simulations or controller design.

Figure 3 summarizes the presented flight dynamics modelling process.

II.A. Aerodynamics

The aerodynamics are modelled using the open-source Athena Vortex Lattice (AVL)[1] potential flow solver. The only input to the aerodynamics estimation are the AVL input files. These describe the airframe geometry as determined from CAD drawings, fotographs or direct measurements. All lifting surfaces are modeled as

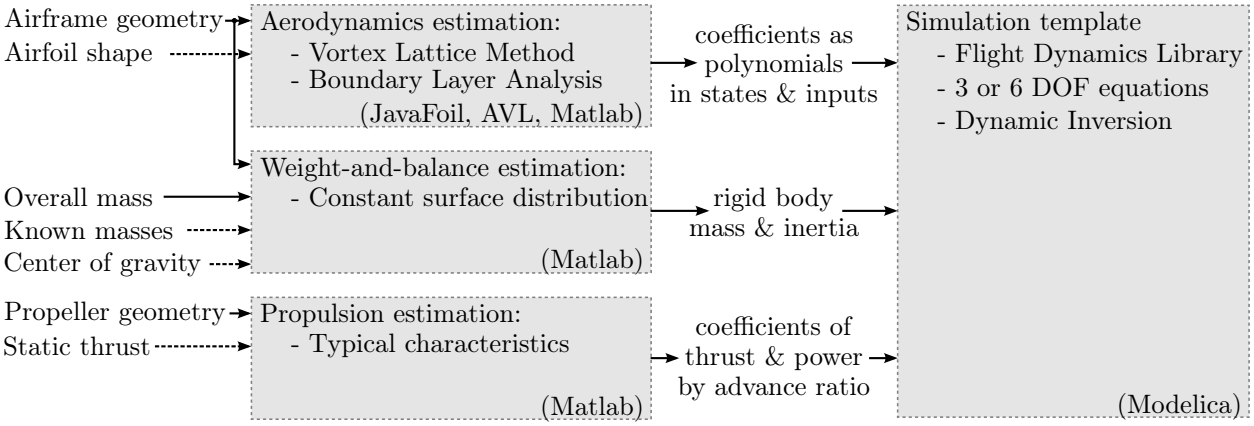

Figure 3. The presented flight dynamics estimation uses very limited geometric information about the aircraft to be modelled. With some easily determined additional measurements (- - -), a reasonable flight dynamics estimation is achieved and used to fill a simulation template based on Modelica and the Flight Dynamics Library.

thin airfoils. Bodies such as the fuselage can be included as slender bodies. AVL allows for defining airfoil shapes by their camber lines and incidence angles.

As the vortex lattice method is a detailled but mostly linear modelling tool, it does includes the induced drag by default. However, additional non-linear drag effects can optionally be included by defining parametric the airfoils' drag coefficient c_D as a parametric function of its lift coefficient c_L. These polars are generated with JavaFoil[6] or a similar two-dimensional aerodynamics solver and then fitted to the AVL parametric representation:

$$
\begin{aligned}
c_D &= f(c_L, c_{L,min}, c_{D,min}, c_{L,0}, c_{D,0}, c_{L,max}, c_{D,max}) \\
&= \begin{cases}
c_{D,min} + const \cdot \frac{c_{L,min} - c_L}{c_{L,min} - c_{L,0}} + const \cdot (c_L - c_{L,min})^2 & \text{for } c_L < c_{L,min}, \\
c_{D,0} + (c_{D,min} - c_{D,0}) \cdot \left(\frac{c_L - c_{L,0}}{c_{L,min} - c_{L,0}} \right)^2 & \text{for } c_L \in [c_{L,min}, c_{L,0}), \\
c_{D,0} + (c_{D,max} - c_{D,0}) \cdot \left(\frac{c_L - c_{L,0}}{c_{L,max} - c_{L,0}} \right)^2 & \text{for } c_L \in [c_{L,0}, c_{L,max}), \\
c_{D,max} + const \cdot \frac{c_{L,max} - c_L}{c_{L,max} - c_{L,0}} + const \cdot (c_L - c_{L,max})^2 & \text{for } c_L \geq c_{L,min}.
\end{cases}
\end{aligned}
$$

This procedure provides fast aerodynamics estimation and does not require extensive modelling. Thus, the aerodynamics model is capable of easily following design and configuration changes, and can provide feedback to the design process in return. It will be shown, that the models obtained by this method provide reasonable estimations of the actual aircraft aerodynamics.

Since AVL is an interactive tool, the computation of the flow field cannot be carried out in real time. The aerodynamics model is thus reduced to a polynomial approximation of the AVL model in an automated process. This process is summarized in Fig. 4.

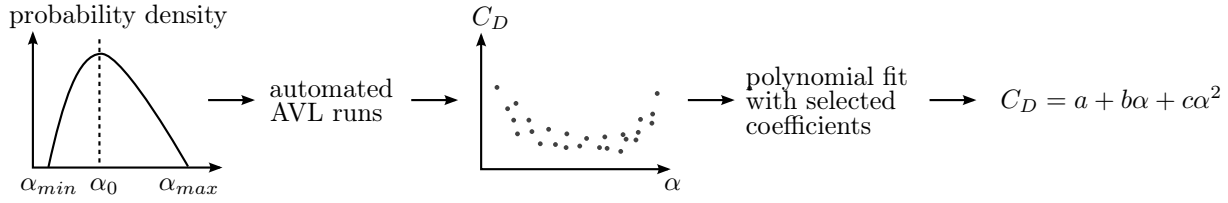

Figure 4. The aerodynamics estimation uses samples of the relevant input variables. In automated AVL runs, a corresponding distribution of the aerodynamic coefficients is produced. The data is reduced using a polynomial fit of the output data on selected factors. The example shown for the drag coefficient C_D dependency on the angle of attack α suggests a quadratic dependency.

In a first step, the AVL model is evaluated at a number of random input points in the relevant flight envelope. A cosine-like probability density distribution concentrated close to the nominal flight conditions proved most reliable, because it increases the validity of the fit in the most relevant flight regime. It can

additionally be bounded to only a defined flight envelope, thereby excluding regions of invalid AVL solutions. However, one must pay attention to the fact that the model will not be valid outside of this envelope.

Convergence studies show that a number of only 100 input samples already provides a reasonable fit. The number of $3^8 = 6561$ input samples would theoretically be sufficient to determine a poylnomial of completely coupled influences for eight input variables up to the power of two. Exceeding this number reduces to fluctuations in the model to less than 1%. A number of 10.000 input samples thus proved largely sufficient to produce a robust fit of the polynomial to the AVL output (see Fig. 5). The overnight calculation takes about 12h on a regular laptop computer for a typical aircraft model with 1.500 panels.

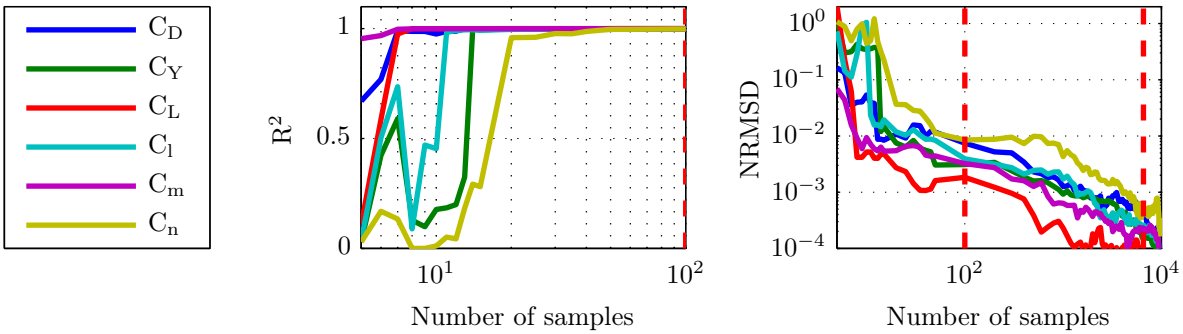

Figure 5. Convergence studies for the polynomial fit used the maximum number of 10.000 samples as the reference. The coefficient of determination R^2 reaches 1 for a number of 100 samples. The root-mean-square deviation normalized by the span of the reference (NRMSD) is less than 1% for this number of samples. Theoretically, a number of $3^8 = 6561$ samples should be sufficient to determine a polynomial containing all possible combinations of the eight influence factors up to the power of two. The NRMSD falls under 0.1% for samples above this number.

The resulting aerodynamic coefficients are then fitted in a least-squares sense with multi-dimensional polynomials $\mathrm{p}(x_1, ..., x_n)$ in the aerodynamic angles (α and β), the dimensionless rotational rates ($\hat{p}, \hat{q}, \hat{r}$) and the aileron, elevator, rudder and flap deflections ($\delta_a, \delta_e, \delta_r, \delta_f$). These polynomials can also cover arbitrary coupling effects by including monomials of the form $x_1^a \cdot ... \cdot x_n^c$.

The relevant monomials are selected by engineering judgement and by inspecting the distribution of the aerodynamics coefficients over the input quantities. Figure 4 e.g. suggests a quadratic dependency of C_D on α. Usually a maximum order of two in each input variable is sufficient for an aerodynamic model close to the nominal flight conditions. The resulting output equations typically have the following form.

$$
\begin{aligned}
C_D &= \mathrm{p}\,(\alpha, \beta, \hat{q}, \delta_e, \delta_f) && \text{(Drag coefficient)} \\
C_L &= \mathrm{p}\,(\alpha, \beta, \hat{q}, \delta_e, \delta_f) && \text{(Lift coefficient)} \\
C_m &= \mathrm{p}\,(\alpha, \beta\hat{q}, \delta_e, \delta_f) && \text{(Pitch moment coefficient)} \\
C_Y &= \mathrm{p}\,(\alpha, \beta, \hat{p}, \hat{r}, \delta_r) && \text{(Side-force coefficient)} \\
C_l &= \mathrm{p}\,(\alpha, \beta, \hat{p}, \hat{r}, \delta_a) && \text{(Rolling moment coefficient)} \\
C_n &= \mathrm{p}\,(\alpha, \beta, \hat{p}, \hat{r}, \delta_r) && \text{(Yaw moment coefficient)}
\end{aligned}
$$

The equations can directly be used to calculate the aerodynamic forces and moments for the aircraft simulation's inputs and states. It completes the first module of the flight dynamics model.

II.B. Weight and Balance

The aircraft geometry description for the aerodynamics estimation is parsed and processed also by a Matlab program, in order to generate a weight-and-balance estimation of the UAV. This estimation evenly distributes the structural mass of the UAV over its surface. It takes into account bodies as hollow hulls and lifting surfaces as flat plates. At least the overall mass of the UAV is needed as an additional input. The process is illustrated along with two suggested refinement steps in Fig. 6.

In a first refinement step, known masses such as the motors, the propellers, the gears, batteries and avionics should be determined and input to the algorithm. The known masses are then subtracted from the total mass and only the remaining mass is distributed over the UAV surface as structural mass.

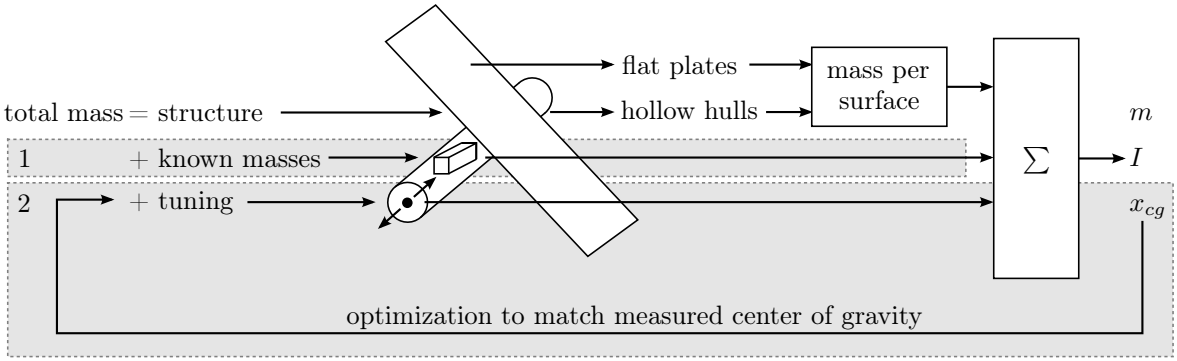

Figure 6. The weight-and-balance estimation evenly distributes the structural mass over the aircrafts' surface. In a first refinement, known mass points can be taken into account. A synthetic mass point can further be used to yield the correct center of gravity.

Another refinement uses the actual center of gravity, which can easily be determined using two scales. A synthetic mass point is then introduced. It can be displaced to manually tune the overall center of gravity to match the measurement. If the pure structural mass is known, the synthetic mass can be determined as the difference between the total mass, the known mass points and the structural mass. This already gives reasonable weight-and-balance estimates, if no mass points are known.

The output of this procedure is mainly an estimated inertia matrix. The overall mass and the center of gravity should match the actually measured data. With these data the aircraft's forces and accelerations can be directly related. It completes the second part of the flight dynamics model.

II.C. Propulsion

The thrust T of a propeller can be calculated using the advance ration J of the propeller and a thrust coefficient c_T, which usually varies with changing advance ratio. In the following equation, ρ is the air density, v the airspeed of the aircraft, RPM the rotations per minute of the propeller and D its diameter:

$$J = \frac{v}{\frac{RPM}{60} D}$$
$$T = c_T(J)\rho \left(\frac{RPM}{60}\right)^2 D^4$$

Most research UAVs use fixed pitch model aircraft propellers for propulsion. For some propellers, there are measurements of the thrust coefficient readily available.[7] For others there are generalized estimations provided by model pilots based on the ratio H/D, with H being the mean pitch of the propeller.[8] This parameter is a defining parameter of most commercial propellers. It is usually known to the user or can simply be measured. A suitable characteristic for the thrust coefficient can then directly be selected in Fig. 7.

However, in order to increase the propulsion model's fidelity, the parameter H/D need not be measured directly. It can be derived from static thrust measurements. The procedure is summarized in Fig. 7. The measured thrust for $J = 0$ is fitted to a parabola in RPM^2, taking into account also an additional constant friction term. From this fit, the static thrust coefficient c_{T0} can be determined. The virtual H/D is then chosen such that it matches the static thrust coefficient. The virtual and the actual mean pitch do not coincide perfectly, but they are reasonably close.

In order to also take into account the propeller torque Q, the empirical finding[9] can be used, that the power coeffcient c_P of a propeller is approximately linear in the thrust coefficient c_T and the advance ratio squared J^2.

$$P = c_P \rho \left(\frac{RPM}{60}\right)^3 D^5 = 2\pi \left(\frac{RPM}{60}\right) Q \tag{1}$$
$$c_P = m c_T + b J^2 \tag{2}$$

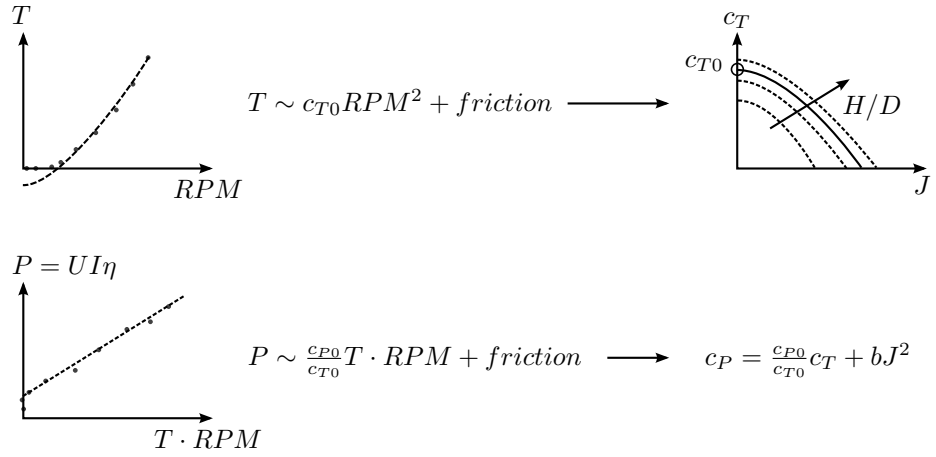

Figure 7. For propulsion estimation, static thrust measurements are used. A parabolic fit of the thrust T to the propeller turn rate RPM yields a static thrust coefficient c_{T0}. This is used for selecting suitable propeller characteristics. The power coefficient is assumed linearly dependent on the thrust coefficient.

The power P can be measured during the static thrust experiments using e.g. the motor current I, voltage U and efficiency η. A linear fit of the power P to the product $T \cdot RPM$ then yields the constant $m = c_{P0}/c_{T0}$ for $J = 0$. The coefficient b has to be estimated or can be neglected for small advance ratios J.

The propulsive forces and moments can now be readily calculated, concluding the flight dynamics estimation routines.

III. Validation

In order to validate the presented flight dynamics estimation routines, they are compared to higher fidelity models. The aerodynamics are compared to the wind-tunnel measured aerodynamics model of the University of Minnesota's FASER aircraft.[10,11] The weight-and-balance estimation is compared to actual inertia measurements of the DLR's ELWIRA aircraft[12] because its payloads are better known. However, the comparison to the FASER weight-and-balance yields similar results for a very rough knowledge about the payloads. Unfortunately, there were no high-fidelity models available for validation of the propulsion estimation. However, the estimation was used in model identification of DLR's Frauke UAV[13] and no noticeable disagreements were found.

III.A. Aerodynamics

The aerodynamics are validated against the non-linear simulation model of the University of Minnesota's FASER aircraft. This reference is derived from wind-tunnel measurements at NASA Langley Research Center and is provided as interpolation tables for the aerodynamics coefficients. The input geometry of the aerodynamics estimation is derived from a rough CAD model provided by the team of the University of Minnesota's UAV laboratory. The resulting AVL model is shown in Fig. 2 on page 2.

In a first step, the AVL model is evaluated at the grid points of the interpolation tables for qualitative comparison of the estimation excluding errors introduced by the polynomial fit. Figure 8 depicts this qualitative comparison as surface plots of the influences included in the non-linear reference model and the estimation's unreduced data. Additional plots are provided in the appendix. The final polynomial reduction is additionally evaluated at the reference's grid points and indicated in the figure as black dots. The choice of coefficients is justified by the very good agreement of the polynomial representation with the original data.

The agreement between the reference and the estimation is mostly reasonable in order of magnitude and sign of the influences. The drag coefficient apparently has to be supplemented by a constant offset in order to match the reference. This can probably be attributed to missing drag contributions in the potential flow solution. The influence of the pitch rate is evidently very different from the reference, which uses a fixed Digital DATCOM[14] estimation for the pitch damping coefficient C_{mq}. As the reliability of this estimation cannot be evaluated, the pitch rate influence is excluded from further comparisons.

The initial comparison plots are then used to select the factors to be included in the polynomial repre-

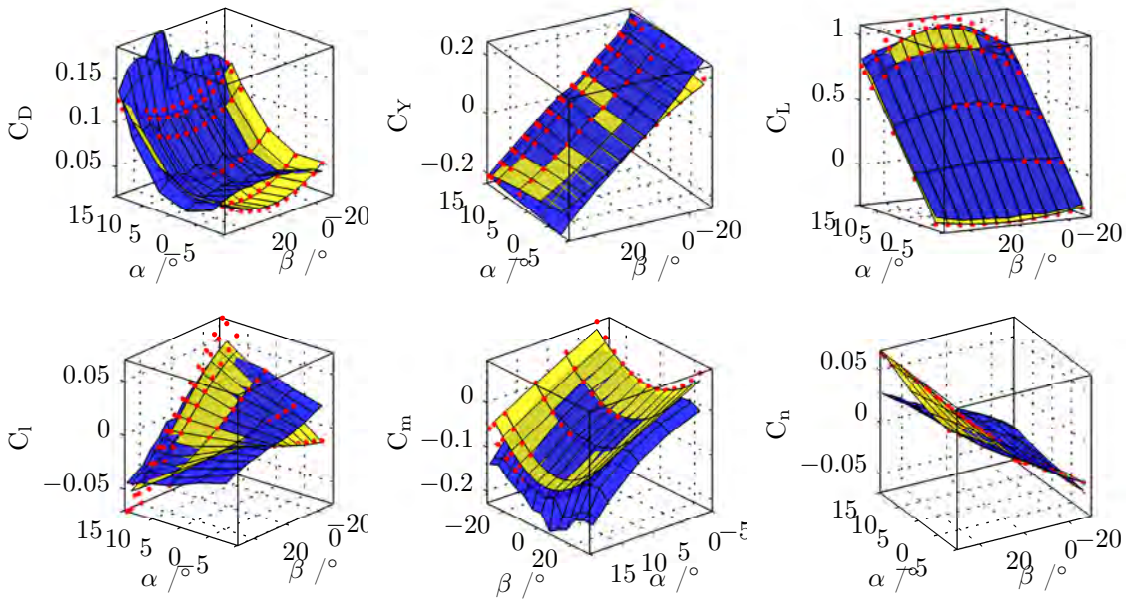

Figure 8. Baseline coefficients of the estimation (yellow) as compared to the reference (blue). The drag coefficient is offset by a constant contribution for small side-slip angles. The polynomial reduction $(\cdot)$ fits the raw data very well. The estimation and the reference agree reasonably well.

sentation. The selected factors are summarized in Table 1. The plots are also used to restrict the range of the input samples to the aerodynamics estimation. These ranges are summarized in Table 2. The ranges are mainly restricted to exclude strong non-linear effects such as stall, and non-smooth influences such as can be seen for the coefficients' differences due to rudder deflections (see Fig. 14 in the appendix).

Table 1. The polynomial aerodynamics model is composed of a linear combination of factors. Variables used include the aerodynamic angles (α and β), the dimensionless rotational rates ($\hat{p}, \hat{q}, \hat{r}$) and the control surfaces ($\delta_a, \delta_e, \delta_r, \delta_f$). The factors are determined by examining Fig. 8.

	const	α	α^2	β	β^2	$\alpha\beta$	$\alpha\beta^2$	$\hat{p}$	$\alpha\hat{p}$	$\hat{r}$	$\alpha\hat{r}$	$\alpha^2\hat{r}$	δ_a	$\alpha\delta_a$	$\beta^2\delta_a$	δ_e	$\alpha\delta_e$	$\alpha^2\delta_e$	δ_r	$\alpha\delta_r$	$\alpha^2\delta_r$	$\beta\delta_r$	$\beta^2\delta_r$	δ_f	$\alpha^2\delta_f$
C_D	✓	·	✓	·	✓	·	·	·	·	·	·	·	·	·	·	✓	✓	·	·	·	·	·	·	✓	✓
C_L	✓	✓	·	·	✓	·	✓	·	·	·	·	·	·	·	·	✓	·	✓	·	·	·	·	·	✓	✓
C_m	✓	✓	·	·	✓	·	·	·	·	·	·	·	·	·	·	✓	·	·	·	·	·	·	·	✓	✓
C_Y	✓	✓	·	✓	·	✓	·	✓	✓	✓	✓	✓	·	·	·	·	·	·	✓	✓	·	✓	✓	·	·
C_l	✓	✓	·	✓	·	✓	✓	✓	·	✓	✓	·	✓	✓	✓	·	·	·	·	·	·	·	·	·	·
C_n	✓	✓	·	✓	·	✓	·	✓	✓	✓	✓	·	·	·	·	·	·	·	✓	✓	✓	✓	✓	·	·

The AVL model is evaluated at 10.000 randomly distributed samples within the ranges shown in Table 2 and fitted with polynomials in the factors shown in Table 1. To evaluate the model fit, an additional number of 1.000 uniformly distributed samples are generated in the ranges provided in Table 2. The polynomial model is evaluated at these samples and compared to the data obtained with the reference model. The overall statistics of this comparison are depicted in Fig. 9. For a detailled discussion of the results, the errors of the fit are included as a function of the input variables in the figures 15, 16, 17, 18, 19, and 20 in the appendix.

The overall model fit is reasonable except for angles of attack just below stall. This is to be expected because of the potential flow model employed. Especially the longitudinal model is in very good agreement with the reference. As noted earlier, an additional constant offset in the drag coefficient is needed to account for unmodelled viscous drag components. The model could be improved in this respect with better drag polars of the airfoils.

The lateral model is also reasonable. Only the yawing moment coefficient has a poor fit to the reference. The yawing moment is generally overestimated. Investigating Fig. 20 reveals that this error is due to a bad estimate of the influence of the side-slip angle β and the rudder deflection δ_r, and possibly an unmatched

Table 2. The AVL model is evaluated in a limited range of the input variables. This range is determined by examining Fig. 8. Main reasons for restrictions are non-linear stall effects or higher order dependencies such as introduced by high rudder deflections.

Input variable	min	nominal	max
$\alpha/^\circ$	-5	0	15
$\beta/^\circ$	-20	0	20
$\hat{p} = pb/2V$	-0.05	0	0.05
$\hat{r} = rb/2V$	-0.1	0	0.1
$\delta_a/^\circ$	-10	0	10
$\delta_e/^\circ$	-10	0	10
$\delta_r/^\circ$	-10	0	10
$\delta_f/^\circ$	0	0	20

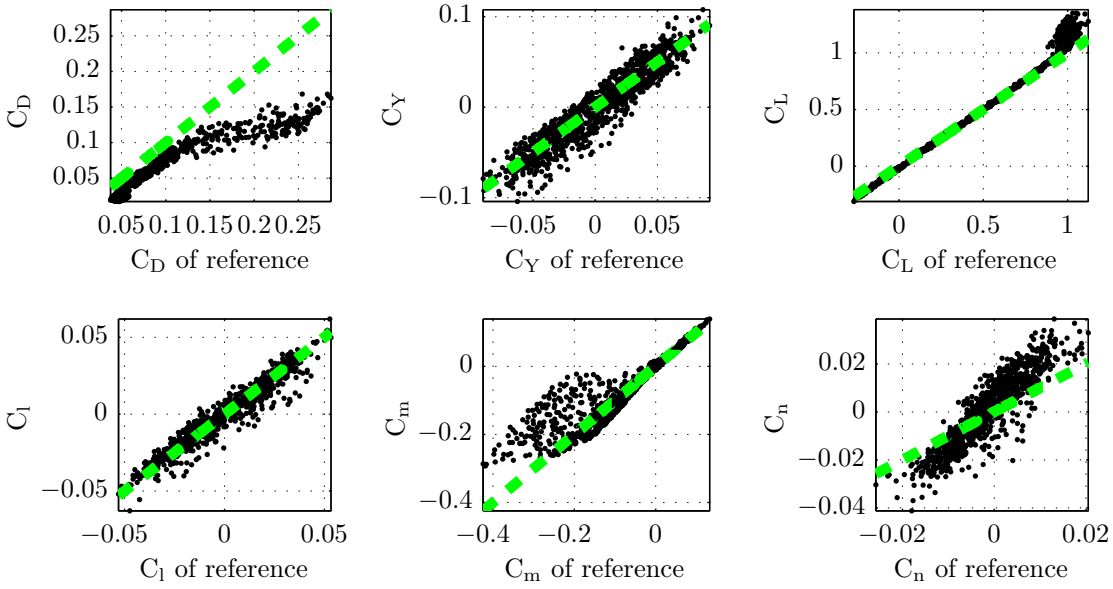

Figure 9. Overall statistics of the polynomial model (·) compared to the reference (– –). The overall model fit is reasonable except for stall regions. The drag coefficient is slightly underestimated and the yaw moment derivatives appear biased.

interaction with effects of the angle of attack α. However, the model of the lateral geometry has a somewhat arbitrary interface between the slender body fuselage and the rudder as a lifting surface. The model could probably be improved at this point.

In summary, the estimation provides reasonable results with coefficients of determination between $R^2 > 0.803$ and $R^2 < 0.985$ for all coefficients. The uncertainty of the model with respect to the data range of the reference is much less than 20% for most of the coefficients except the yaw moment coefficient C_n. However, the quality of the model can probably be improved by a more elaborate representation of the aircraft geometry in the potential flow solver.

III.B. Weight and Balance

The weight-and-balance estimation is validated for the ELWIRA aircraft using a pendulum to measure the aircraft's actual inertia. The overall mass and center of gravity do not need to be verified, because they are measured inputs to the estimation routine. The inertia estimates are obtained using the procedure described in Sec. II.B. The overall mass of the aircraft is 36 kg. 21 distinct mass points are included in the estimation, accounting for 70 % of the total mass. The trim mass of 2.5 kg as used in the actual aircraft configuration is used for tuning the center of gravity to match $x_{cg} = 0.95\,\mathrm{m}$.

The experimental set-up for the inertia measurements is depicted in Fig. 10. A torsion spring is fixed to axis 6 of a KUKA KR 500 industrial manipulator. ELWIRA is attached to the other end of the spring and can now oscillate around the spring axis. The additional mounting structure is made of Item profiles and must be corrected for in order to yield the correct aircraft inertia.

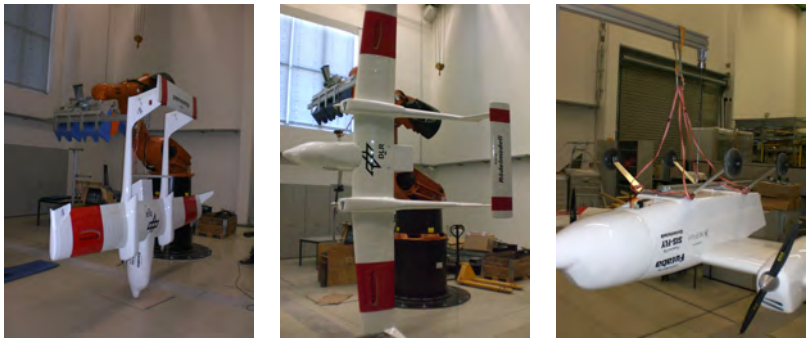

(a) X axis (b) Y axis (c) Z axis

Figure 10. The pendulum set-up for the weight-and-balance inertia measurements consists of a KUKA KR-500 industrial manipulator holding a torsional spring. The ELWIRA aircraft is fixed to this spring and can oscillate around the spring axis as indicated in the figure.

The torsion spring used for the experiments is a cylindrical steel bar with a diameter of $d = 4\,\mathrm{mm}$ and a length of $l = 0.6\,\mathrm{m}$. Assuming an approximate shear modulus of $G = 79.3\,\mathrm{GPa}$, its torsional stiffness is estimated to $\overline{C} = G\pi d^4/32L \approx 3.322\,\mathrm{N\,m/rad}$ according to handbook formulas.[15]

The aircraft's inertia is measured about its three body axes to yield its main inertia elements I_{xx}, I_{yy}, and I_{zz}. The inertia tensor's coupling terms I_{xy}, I_{xz} and I_{yz} are assumed to be zero during the measurements. This assumption is not true for a general aircraft. But if the centre of gravity is located in a symmetry plane at $y = 0$, the two terms I_{xy} and I_{yz} are actually zero by definition. I_{xz} typically is one order of magnitude lower than the main inertia elements and is neglected in this validation.

The pedulum set-up depicted in Fig. 10 can be described by the ODE for a damped harmonic oscillator:

$$I\ddot{\varphi}(t) = -C\varphi(t) - D\dot{\varphi}(t)$$

In this equation, φ, $\dot{\varphi}$ and $\ddot{\varphi}$ are the rotation angle and its temporal derivatives, I is the inertia element about the rotation axis, C is the torsion spring's stiffness and D is the linear damping coefficient. The analytical solution to this ODE is

$$\varphi(t) = \varphi_0 e^{-t/\tau}\cos(\omega t), \qquad \text{with} \quad \omega = \omega_0\sqrt{1-\zeta^2},$$
$$\dot{\varphi}(t) = \dot{\varphi}_0 e^{-t/\tau}\sin(\omega t), \qquad \tau = \frac{1}{\zeta\omega_0}.$$

To calculate the angular frequency ω and the time constant τ of this system, the damping ratio ζ and the natural (or undamped) angular frequency of the system ω_0 are needed:

$$\omega_0 = \sqrt{C/J},$$
$$\zeta = \frac{D}{2J\omega_0}.$$

If ζ is small, the damped angular frequency ω and the natural angular frequency ω_0 are almost equal. It then suffices to measure $\omega \approx \omega_0$ to determine either the spring constant C or the inertia I, if the other is known. The spring constant is thus calibrated using a well-known reference object. It is then assumed to remain constant during the following experiments and the inertia of the aircraft can be determined. In this study, the maximum damping coefficient was $\zeta < 0.1$. The maximum error introduced by the assumption of $\zeta \approx 0$ is about 0.5%.

Three methods are applied to extract the inertia from the measurements: Stop-watch measurements of the oscillation period, fourier transformation of the angular rates measured by the onboard inertial measurement unit, and numerically fitting the oscillation's ODE to the sensor data. The variances from all methods are at maximum in the range of 5% of the mean values. Stop-watch measurements yielded the second-best variances. Only a non-linear optimization of the ODE performed better, but is much more complicated. The stop-watch measurements are thus used for the following calculations.

The inertia measurements are summarized in Table 3. The spring constant is close to the expected value. The raw inertia measurements are corrected for the raw inertia of the mounting structure. An additional correction accounts for a shift in center of gravity between the two raw measurements. The measurement uncertainty is given as the 99.7% confidence interval, i.e. three times the standard deviation. One can see a very good agreement of the estimates with the measurements. The maximum error is 7.3 % in the z-axis estimation. This is a very close match given the simplicity of the estimation routine.

Comparisons of the FASER inertia matrix yields similar results. The aircraft's weight and balance is modelled with the sole knowledge of the total mass 7.41 kg and the empty weight of the aircraft. A synthetic mass point of 4.28 kg accounts for the payload mass and is used to tune the center of gravity to $x_{cg} = 0.315\,\mathrm{m}$. The resulting inertia estimation is $I_{xx} = 0.6127\,\mathrm{kg\,m^2}$, $I_{yy} = 0.9114\,\mathrm{kg\,m^2}$ and $I_{zz} = 1.4883\,\mathrm{kg\,m^2}$. This is a very close match to the reference data given as $I_{xx} = 0.7646 \pm 0.0922\,\mathrm{kg\,m^2}$, $I_{yy} = 0.9495 \pm 0.0601\,\mathrm{kg\,m^2}$, and $I_{zz} = 1.6393 \pm 0.0612\,\mathrm{kg\,m^2}$.

IV. Conclusions

An algorithm is presented, which is able to derive reasonable flight dynamics models from geometry data and few additional pieces of information. In the presented example, the aerodynamic model has errors of much less than 20% of the reference's data range. Only the yawing moment is generally overestimated. More elaborate modelling might alleviate this discrepancy. The inertia estimate is accurate to within 10%. Even for a very rough knowledge about the aircraft's mass properties, a very good estimate is achieved.

The models are simple to generate and can thus be adapted to changing configurations easily. This is especially valueable for small teams operating a multitude of different fixed-wing UAVs. The implementation using Modelica is advantageous because of its modularity and the possibility to easily derive model variants such as non-linear dynamic inverse models.[4]

Further extensions of the estimation routines will include in-house aerodynamics estimation[16] and integration with more detailled flight dynamics modelling.[17] First approaches to model the stall characteristics use rough a-posteriori alterations of the original polynomial model according to the XPlane approach.[18] Better estimations might be achieved combining blade element theory with vortex lattice models.

Table 3. After calibration of the torsional spring, the three main entries of the inertia matrix are determined. The raw data has to be corrected for an Item mounting structure. An additional correction term accounts for different measuring axes of the aircraft inertia and the mounting inertia. The negative correction term in I_{yy} is due to an additional mass involved in the measurement of the correction. The overall agreement of the estimation with the reference is within 10% of the measured inertias.

	$\overline{\omega}_0$	$3\sigma_\omega$	$\overline{J}$	$3\sigma_J$	$\overline{C}$	$3\sigma_C$
Reference inertia			**0.126**	**0.001**		
Spring calibration	4.958	0.073	0.126	0.001	**3.101**	**0.123**
Spring estimation					3.322	
Inertia X raw	0.552	0.039	**10.167**	**1.848**	3.101	0.123
- Correction X raw	3.679	0.049	0.229	0.015	3.101	0.123
- Correction X CG			0.000	0.000		
Inertia X			**9.938**	**1.863**		
Inertia X estimate			**11.029**			
Inertia Y raw	0.514	0.007	**11.719**	**0.801**	3.101	0.123
- Correction Y raw	1.066	0.015	2.729	0.185	3.101	0.123
- Correction Y CG			-0.471	0.101		
Inertia Y			**9.460**	**1.087**		
Inertia Y estimate			**9.800**			
Inertia Z raw	0.387	0.003	**20.752**	**1.090**	3.101	0.123
- Correction Z raw	5.631	0.051	0.098	0.006	3.101	0.123
- Correction Z CG			0.023	0.000		
Inertia Z			**20.631**	**1.096**		
Inertia Z estimate			**19.381**			

Appendix

This appendix provides additional validation figures for the aerodynamics model.

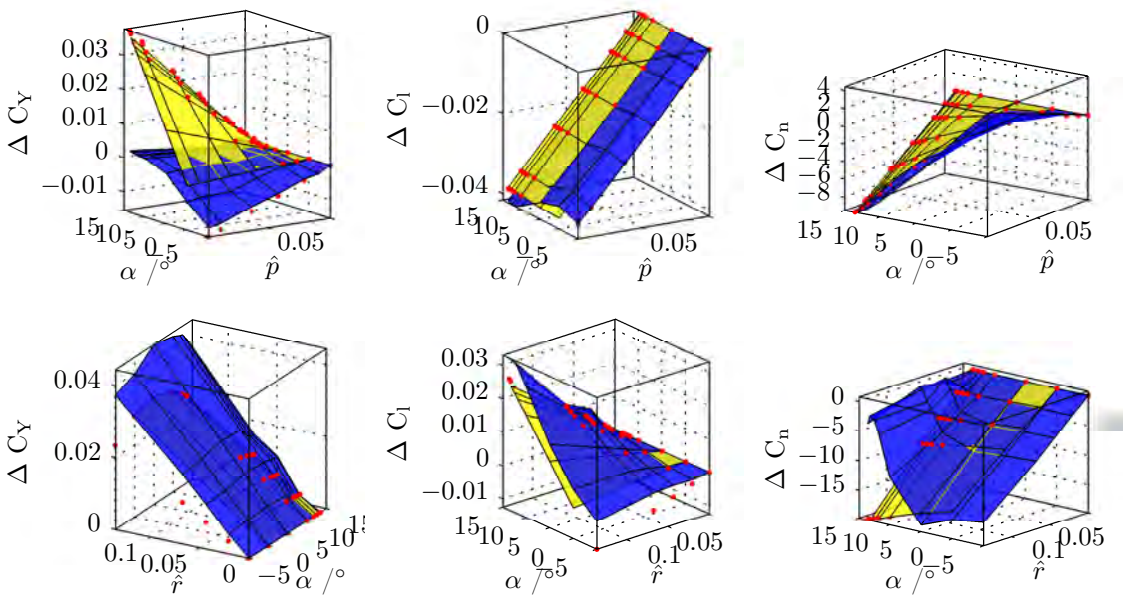

Figure 11. Initial comparison of the roll and yaw rate influences on the aerodynamic coefficients. The estimation (yellow) fits the reference (blue) resonably well for small values of the input variables. The polynomial fit $(\cdot)$ to the estimation data is good.

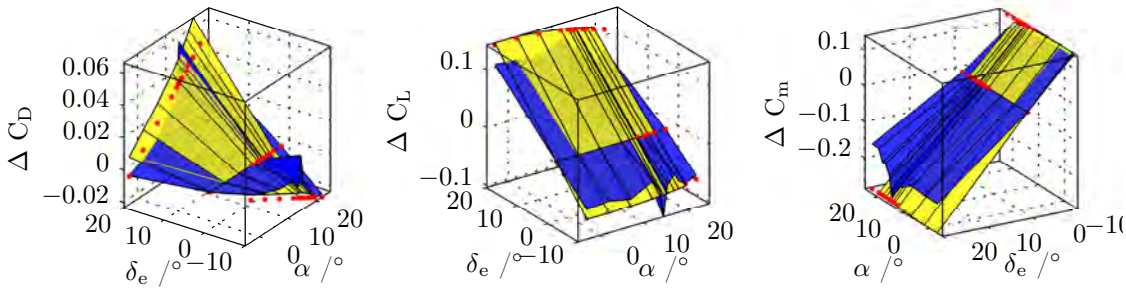

Figure 12. Initial comparison of the elevator influences on the aerodynamic coefficients. The estimation (yellow) fits the reference (blue) resonably well for small values of the input variables. The polynomial fit $(\cdot)$ to the estimation data is good.

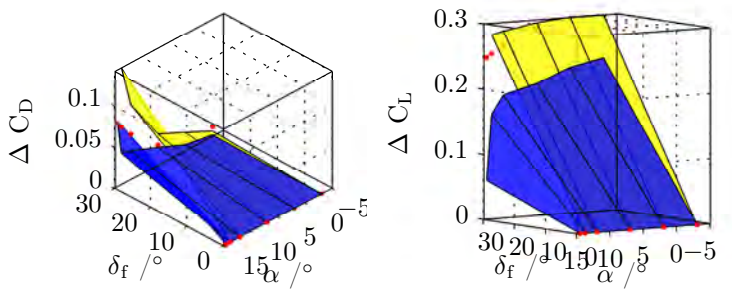

Figure 13. Initial comparison of the flap influences on the aerodynamic coefficients. The estimation (yellow) fits the reference (blue) resonably well for small values of the input variables. The polynomial fit (·) to the estimation data is good.

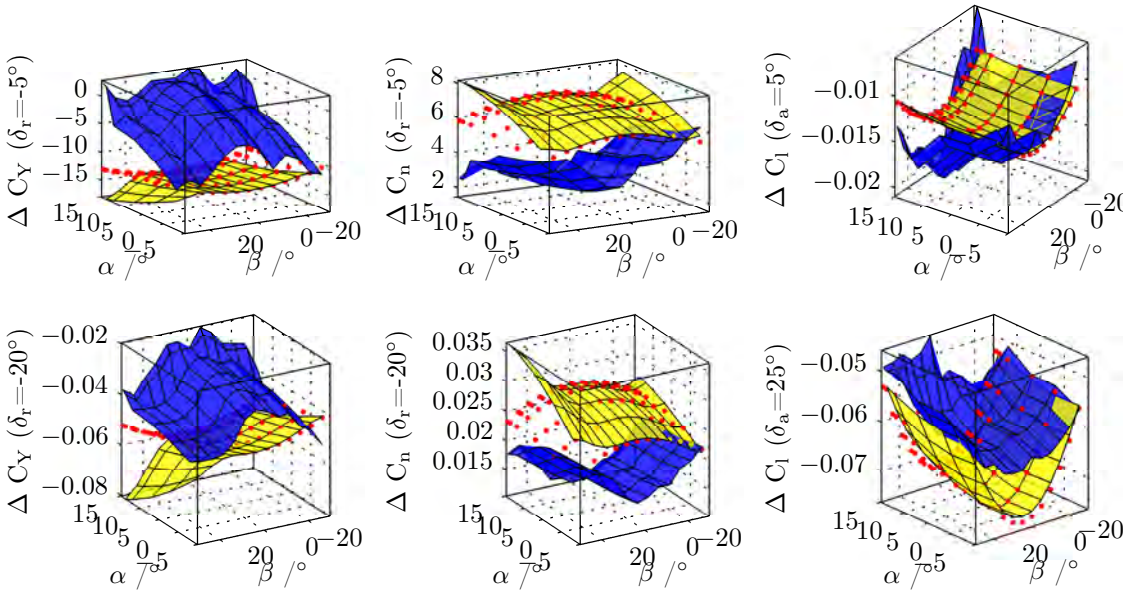

Figure 14. Initial comparison of the rudder and aileron influences on the aerodynamic coefficients. There are noticeable differences between the estimation (yellow) fits the reference (blue) resonably well for small values of the input variables. The polynomial fit (·) to the estimation data is good.

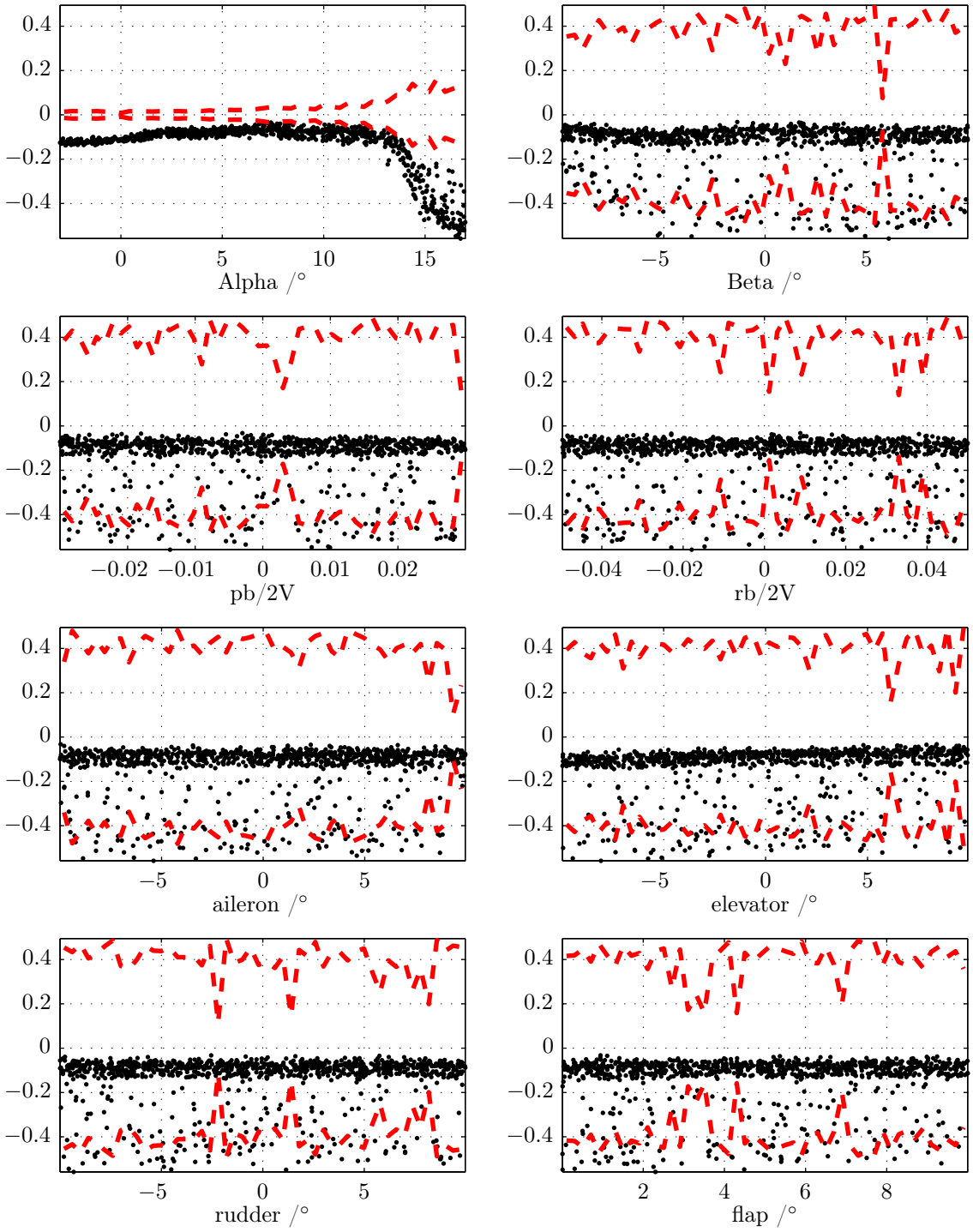

Figure 15. Error statistics of the estimated drag coefficient C_D (·) are plotted as a function of the input variables. The estimation is sampled at 1.000 random points and compared to the reference. It is scaled to the span of the reference data. The maximum deviations in the reference are included for comparison (– –). They are obtained by determining the minimum and maximum values, while keeping one input variable constant. The overall model fit is good except for stall, which is not modelled by AVL. The main influence factor is the angle of attack. The drag is globally underestimated because of missing drag components in the potential flow model. Additional noticeable error trends stem from a slight offset of the elevator influence.

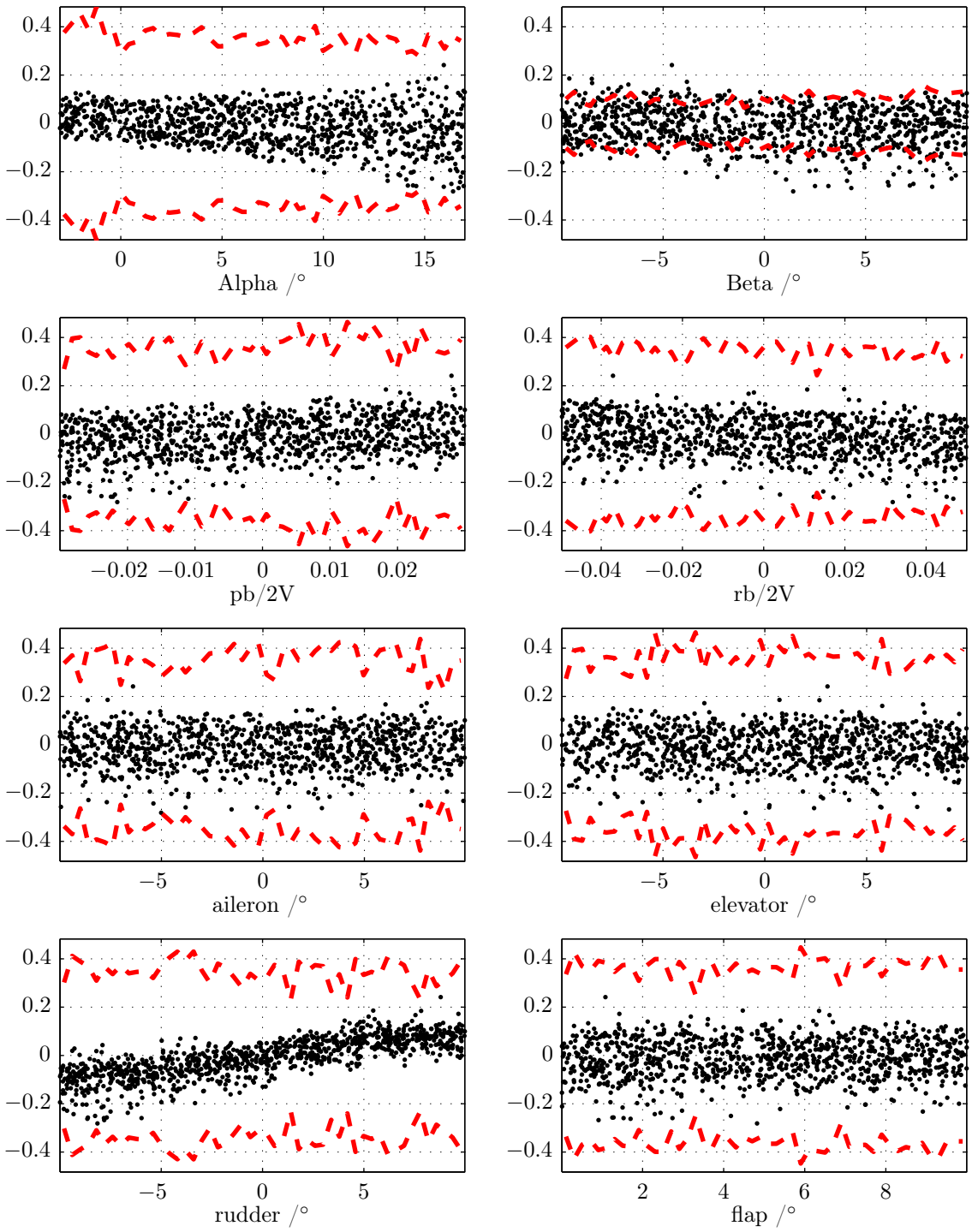

Figure 16. Error statistics of the estimated side force coefficient C_Y (·) are plotted as a function of the input variables. The estimation is sampled at 1.000 random points and compared to the reference. It is scaled to the span of the reference data. The maximum deviations in the reference are included for comparison (– –). They are obtained by determining the minimum and maximum values, while keeping one input variable constant. The overall model fit is reasonable. There is a slight mismatch in the roll and yaw rate influences and an additional cubic rudder influence is suggested by the results. The increasing error for higher angles of attack probably stems from unmodelled stall effects or reduced rudder efficiency in the wing's wake.

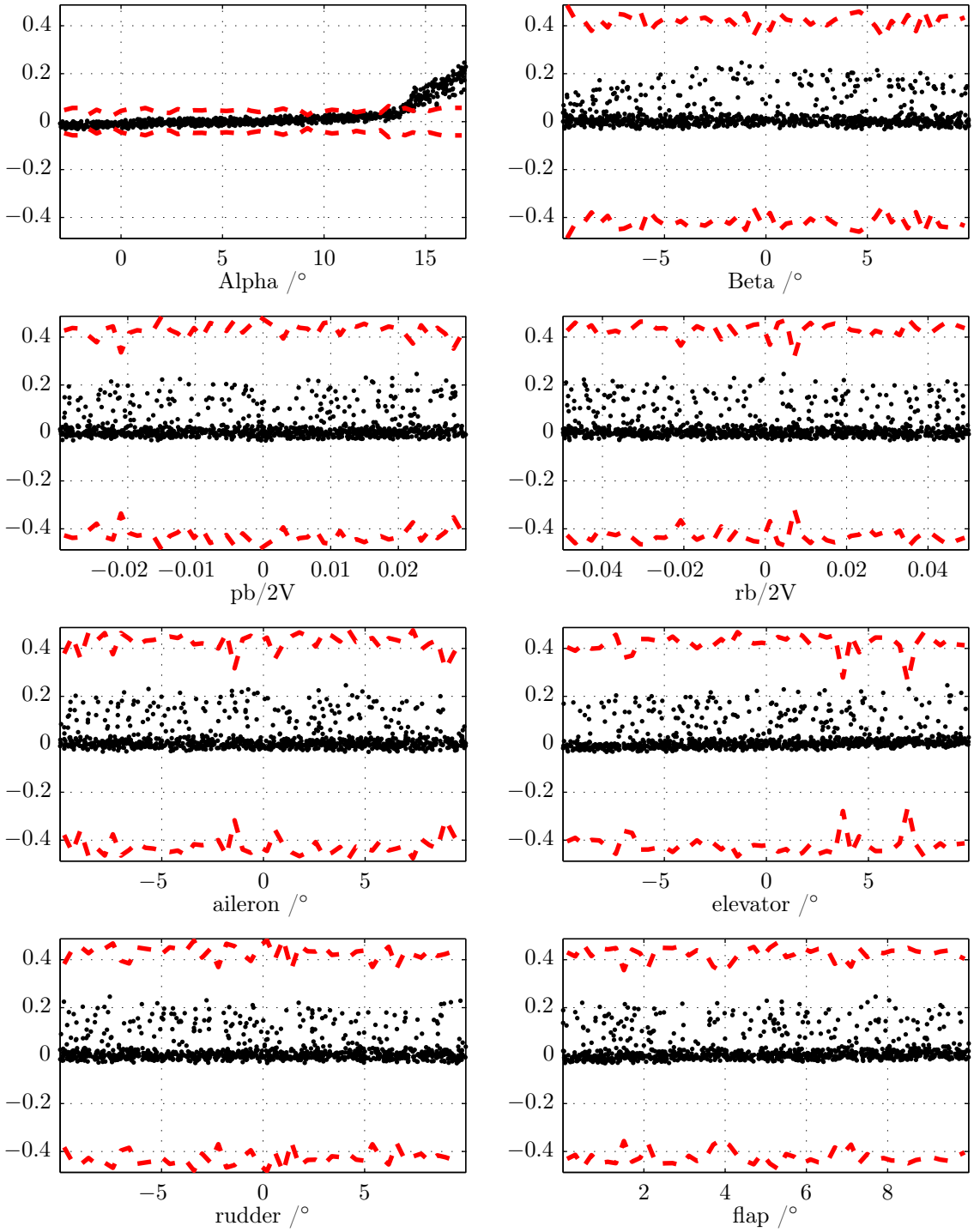

Figure 17. Error statistics of the estimated lift coefficient C_L $(\cdot)$ are plotted as a function of the input variables. The estimation is sampled at 1.000 random points and compared to the reference. It is scaled to the span of the reference data. The maximum deviations in the reference are included for comparison (– –). They are obtained by determining the minimum and maximum values, while keeping one input variable constant. The overall model fit is very good. The main influence factor is the angle of attack. The corresponding linear influence is slightly offset. Larger errors stem from stall effects, which are not modelled.

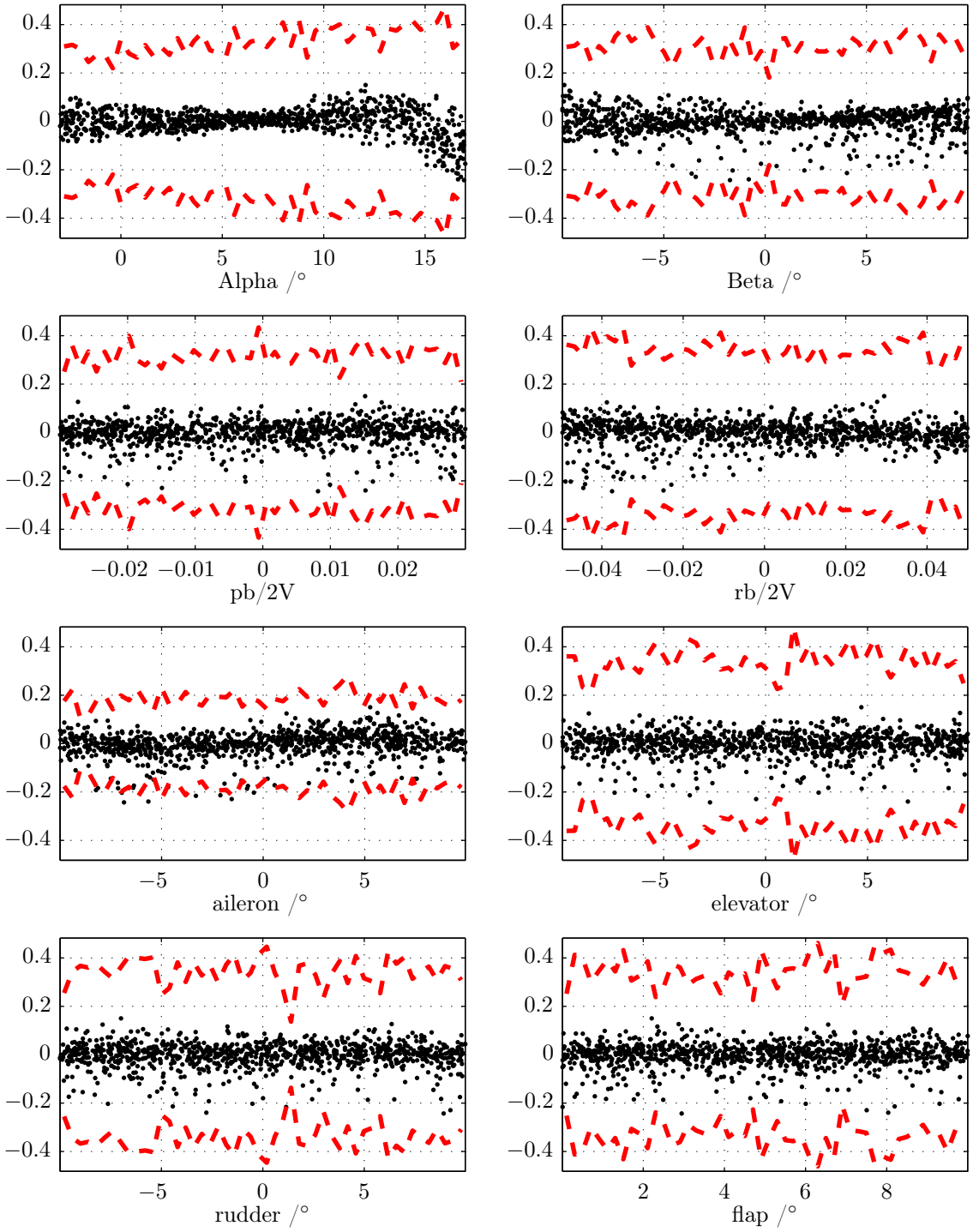

Figure 18. Error statistics of the estimated rolling moment coefficient C_l (·) are plotted as a function of the input variables. The estimation is sampled at 1.000 random points and compared to the reference. It is scaled to the span of the reference data. The maximum deviations in the reference are included for comparison (– –). They are obtained by determining the minimum and maximum values, while keeping one input variable constant. The overall model fit is good. The main influence of the aileron is captured resonably well. The best fit is found for zero side-slip and angles of attack close to 5°.

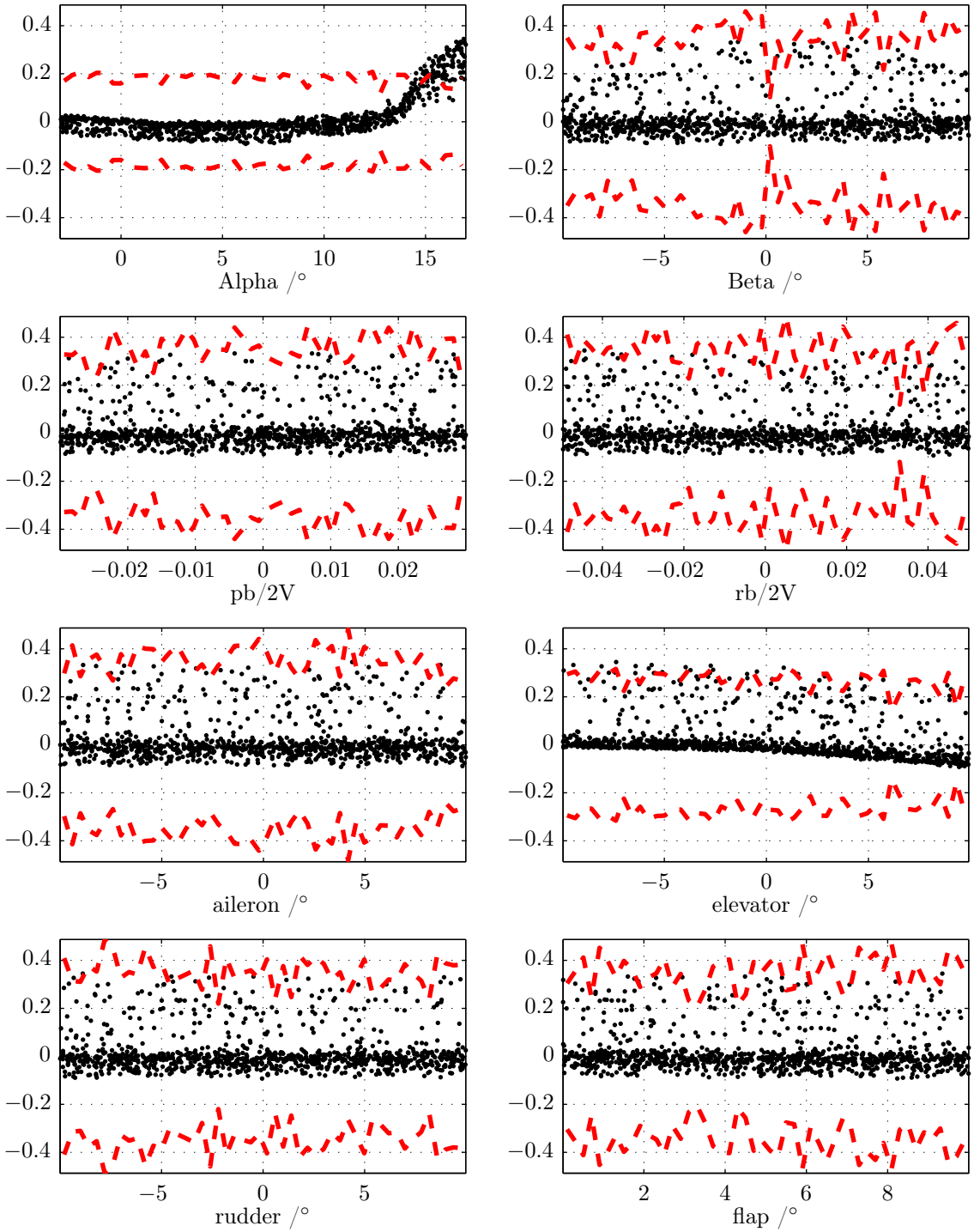

Figure 19. Error statistics of the estimated pitching moment coefficient C_m (·) are plotted as a function of the input variables. The estimation is sampled at 1.000 random points and compared to the reference. It is scaled to the span of the reference data. The maximum deviations in the reference are included for comparison (– –). They are obtained by determining the minimum and maximum values, while keeping one input variable constant. The overall model fit is good. The main influence is due to the angle of attack. The error statistics suggest an additional quadratic dependency here. There is a slight offset in the effect of the elevator. Larger errors are due to unmodelled stall.

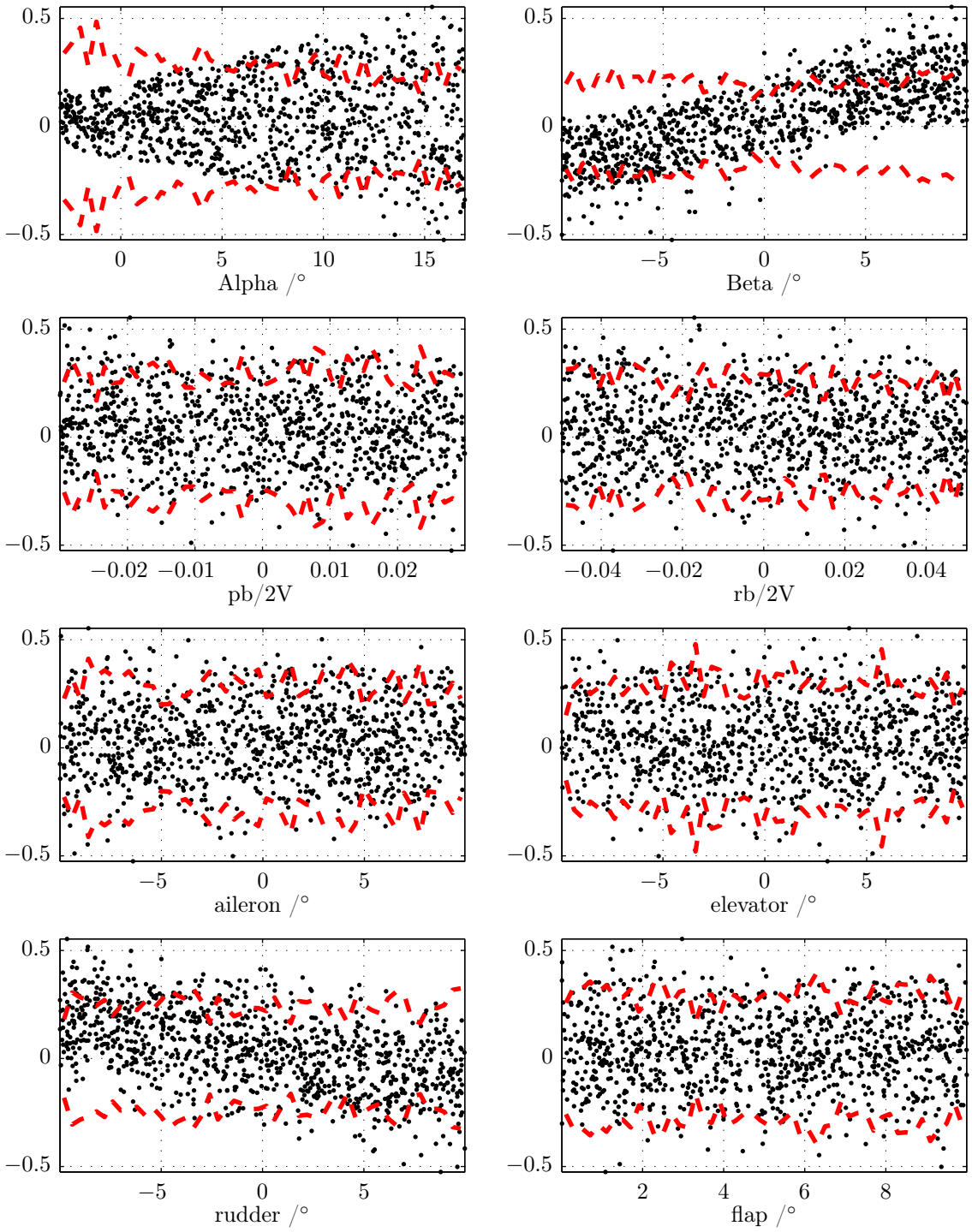

Figure 20. Error statistics of the estimated yawing moment coefficient C_n (·) are plotted as a function of the input variables. The estimation is sampled at 1.000 random points and compared to the reference. It is scaled to the span of the reference data. The maximum deviations in the reference are included for comparison (– –). They are obtained by determining the minimum and maximum values, while keeping one input variable constant. The overall model fit is poor. The main influence of the side-slip angle is noticeably offset. The influence of the rudder is not covered very well. Larger errors are introduced at high angles of attack. The errors might be due to coupling with the angle of attack, such as reduced tail efficiency in the wing's wake..

References

[1]Drela, M. and Youngren, H., "Athena Vortex Lattice," online at http://raphael.mit.edu/avl, September 2004.

[2]Owens, D. B., Cox, D. E., and Morelli, E. A., "Development of a low-cost sub-scale aircraft for flight research: The FASER project," *25th AIAA Aerodynamic Measurement Technology and Ground Testing Conference*, No. 2006-3306, 2006.

[3]Looye, G., "The new DLR flight dynamics library," *Proceedings of the 6th International Modelica Conference*, Vol. 1, 2008, pp. 193–202.

[4]Klöckner, A., Leitner, M., Schlabe, D., and Looye, G., "Integrated Modelling of an Unmanned High-Altitude Solar-Powered Aircraft for Control Law Design Analysis," *CEAS EuroGNC*, edited by Q. Chu, B. Mulder, D. Choukroun, E.-J. van Kampen, C. de Visser, and G. Looye, Vol. Advances in Aerospace Guidance Navigation and Control – Selected Papers of the Second CEAS Specialist Conference on Guidance, Navigation and Control, Springer Berlin Heidelberg, Delft, The Netherlands, 10-12 April 2013 2013, pp. 535–548.

[5]Fritzson, P., *Principles of object-oriented modeling and simulation with Modelica 2.1*, Wiley-IEEE Press, 2004.

[6]Hepperle, M., *JAVAFOIL User's Guide*, 2011.

[7]Brandt, J. and Selig, M., "Propeller Performance Data at Low Reynolds Numbers," *AIAA Paper*, Vol. 1255, 2011, pp. 49.

[8]Hildebrandt, G., "Wirkungsgrad des Propellers," online: http://home.arcor-online.de/guenter22/doc/propeller.pdf, online: http://home.arcor-online.de/guenter22/doc/propeller.pdf.

[9]Lowry, J. T., *Propeller Aircraft Performance and The Bootstrap Approach*, Aeronautics Learning Laboratory for Science, Technology, and Research, April 1999, online http://www.allstar.fiu.edu/aero/BA-Form&gra.htm.

[10]Morelli, E. A. and DeLoach, R., "Wind tunnel database development using modern experiment design and multivariate orthogonal functions," *Proceedings of the 41st Aerospace Sciences Meeting and Exhibit*, Vol. 653, AIAA, 2003.

[11]Hoe, G., Owens, D. B., and Denham, C., "Forced Oscillation Wind Tunnel Testing for FASER Flight Research Aircraft," *Atmospheric Flight Mechanics Conference*, AIAA, Minneapolis, MN, 13-16 Aug 2012, NF1676L-14053.

[12]Klöckner, A., "ELWIRA – Flying robot platform for control, guidance and mission experiments," *UAV World*, Frankfurt a.M., Germany, November 03 2010.

[13]Lombaerts, T., "Aerodynamic model identification of Frauke UAV," *AIAA Atmospheric Flight Mechanics Conference*, AIAA, AIAA, Minneapolis, Minnesota, USA, 13-16 Aug 2012, AIAA-2012-4512.

[14]Williams, J. E. and Vukelich, S. R., "The USAF Stability and Control Digital DATCOM. Volume I. Users Manual," Tech. rep., US Air Force Flight Dynamics Lab, 1979, AFFDL-TR-79-3032.

[15]Knaebel, M., Jäger, H., and Mastel, R., *Technische Schwingungslehre*, Vieweg+Teubner Verlag | GWV Fachverlage GmbH, Wiesbaden, 2009, ISBN 978-3-8351-0180-7.

[16]Kier, T.M. and Looye, G.H.N., "Unifying Manoeuvre and Gust Loads Analysis," *International Forum on Aeroelasticity and Structural Dynamics*, 2009, IFASD-2009-106.

[17]Kuchar, R., "An Integrated Data Generation Process for Flight Dynamics Modeling in Aircraft Design," *DLRK*, Deutsche Gesellschaft für Luft- und Raumfahrt e.V. (DGLR), Berlin, Germany, 10.-12. Oct. 2012.

[18]Laminar Research, "Supplement: Airfoil-Maker. Designing an Airfoil," *X-Plane Wiki*, Laminar Research, 2013, http://wiki.x-plane.com/Supplement:_Airfoil-Maker#Designing_an_Airfoil. Access 17 July 2013.